energies

MDPI

Article

A Comparative Investigation on Solar PVT- and PVT-PCM-Based Collector Constancy Performance

MD Shouquat Hossain [1,*], Laveet Kumar [2], Adeel Arshad [3,*], Jeyraj Selvaraj [4], A. K. Pandey [5,6] and Nasrudin Abd Rahim [4]

1 School of Chemistry and Chemical Engineering, Institute for Energy Research, Jiangsu University, Zhenjiang 212013, China
2 Department of Mechanical Engineering, Mehran University of Engineering and Technology, Jamshoro 76090, Pakistan
3 Environment and Sustainability Institute, Faculty of Environment, Science and Economy, University of Exeter, Penryn Campus, Penryn Cornwall TR10 9FE, UK
4 Higher Institution Centre of Excellence (HICoE), UM Power Energy Dedicated Advanced Centre (UMPEDAC), University of Malaya, Kuala Lumpur 59990, Malaysia
5 Research Centre for Nano-Materials and Energy Technology (RCNMET), School of Science and Technology, Sunway University, No. 5, Jalan Universiti, Bandar Sunway, Petaling Jaya 47500, Malaysia
6 CoE for Energy and Eco-Sustainability Research, Uttaranchal University, Dehradun 248007, India
* Correspondence: shouquat64@gmail.com (M.S.H.); a.arshad@exeter.ac.uk (A.A.)

Abstract: Solar photovoltaic (PV) technology has a lower adoption rate than expected because of different weather conditions (sunny, cloudy, windy, rainy, and stormy) and high material manufacturing costs. To overcome the barriers to adoption, many researchers are developing methods to increase its performance. A photovoltaic–thermal absorber hybrid system may shift its performance, but to become more efficient, the technology could improve with some strong thermal absorber materials. A phase change material (PCM) could be a suitable possibility to enhance the (electrical and thermal) PV performance. In this study, a solar PVT hybrid system is developed with a PCM and analyzed for comparative performance based on Malaysian weather conditions. The result shows PV performance (both electrical and thermal) was increased by utilizing PCMs. Electrical and thermal efficiency measurements for different collector configurations are compared, and PV performance and temperature readings are presented and discussed. The maximum electrical and thermal efficiency found for PVT and PVT-PCM are 14.57% and 15.32%, and 75.29% and 86.19%, respectively. However, the present work may provide extensive experimental methods for developing a PVT-PCM hybrid system to enhance electrical and thermal performance and use in different applications.

Keywords: solar photovoltaic; phase change material; photovoltaic-thermal absorber; electrical performance; thermal performance

Citation: Hossain, M.S.; Kumar, L.; Arshad, A.; Selvaraj, J.; Pandey, A.K.; Rahim, N.A. A Comparative Investigation on Solar PVT- and PVT-PCM-Based Collector Constancy Performance. *Energies* **2023**, *16*, 2224. https://doi.org/10.3390/en16052224

Academic Editor: Kamel Hooman

Received: 21 December 2022
Revised: 20 February 2023
Accepted: 21 February 2023
Published: 25 February 2023

1. Introduction

In recent years, solar energy applications have grown rapidly to meet strict environmental protection requirements and electricity demands. Renewable energy sources such as solar, wind, biogas, biomass, hydropower, and geothermal energy offer highly promising CO_2-free alternatives. Since the 1970s, much research and development have been done on photovoltaic thermal systems. Many innovative designs and products have already been forwarded for quality evaluation by academics and professionals alike [1]. In the 1980s, research works focused mainly on flat-plate collectors. Researchers/professionals performed an analysis of light concentration PVT systems [2–5]. In the late 1980s, for about 10 years, Garg et al. (1994) [6] and some researchers performed detailed analyses of the thermal efficiency of hybrid PVT air and liquid heating systems [7–9]. The thermal efficiency calculation of a flat-plate collector with the use of a modified Hottel–Whillier model was also performed [10,11]. In the mid-1990s, work started in various parts of the

world on creating models for various types of PV and thermal blend systems [1]. Many theoretical and experimental studies of PVT were conducted with either water or air as the coolant [12–16]. A single PV system can produce about 38% electricity, depending on the location [17].

The early PVT system used air, water, or evaporative collectors with monocrystalline, polycrystalline, or amorphous silicon (c-Si, pc-Si, or a-Si) or thin-film solar cells; flat-plate or concentrator types; glazed or unglazed panels; natural or forced fluid flow; stand-alone or building-integrated features; etc. [18,19] At the point when the PV module was operated under dynamic cooling conditions, the temperature dropped appreciably, yet the efficiency of the solar cells managed to increase between 12% and 14% [20]. The total energy-saving efficiency of the PVT collector without and with reflectors is found to be 60.1% and 46.7%, respectively. The thermal efficiency improved by approximately 80%, while at the same time cooling of the PV cells was made possible [21,22]. The solar panel can also increase the temperature, which can cause serious degradation and shorten the lifespan of the PV cells. Among those technologies or designs, the systems of the utilization of air, liquid, heat pipes, PCM, and thermoelectric (TE) devices not only aid the cooling of PV cells but also supply useful heat energy for many applications [23]. The main barrier to implementing solar energy is its irregular supply.

In solar power systems, there is always a detachment between demand and supply, which can be mitigated to some extent through the use of effective energy storage materials, such as phase change materials (PCMs). Phase change materials (PCMs) are widely used as thermal energy storage (TES) agents because they can store and release a significant amount of energy during the phase change process [24]. These substances do not release sensible heat during phase transitions; instead, they absorb latent heat from the environment, which is an endothermic process. Over a certain temperature range, PCMs have the ability to absorb and store energy. PCMs can accumulate 5–14 times more energy per unit volume than water, concrete, or rock [24]. Through the storage of large amounts of heat, these materials can extend the heat availability period [25]. However, these materials were not tried in thermal energy storage before the mid-1970s [26]. In fact, the world energy crisis of that decade prompted research on thermal energy storage, where PCMs came out as the most promising alternative. One of the earliest uses of PCMs in the PV system temperature regulation was reported in 1978 [27]. Huang et al. (2004) [28] first attempted the application of PCMs in the thermal regulation of photovoltaic systems. Thereupon, Hasan et al. (2010) [29], Browne et al. (2016) [30], Sharma et al. (2016) [31], and many other researchers worked on integrating PCMs into controlling PV cell temperature and solar energy storage.

To enable rapid and aggregate phase changes, PCMs are typically housed in thermally conductive metal casings and joined on the PV backside using thermal paste [32]. A non-uniform temperature distribution throughout the solar cells is caused by two complex issues with PCM casings or boxes: (1) an irregular solidification pattern of the material from the liquid phase and uneven distribution inside the box; and (2) inhomogeneous and unsound contact between the PV backside and the PCM container, which results in poor heat transfer from the solar cells to the PCM. The main issue with using PCMs in PV thermal regulation, however, is that they have poor thermal conductivity, low specific heat, and a wide range of phase transitions. Despite the fact that most PCMs have high latent heat, which helped them become popular in thermal storage applications, most of them have low thermal conductivity, which makes it difficult to transfer heat effectively and delays the phase transition of the solar cell temperature.

In addition, the majority of PCMs, particularly the organic (carbon-bearing) ones, have specific heats that are significantly lower than those of water, which shows that they are unable to store a large amount of heat. Another problem with organic PCMs is that they start transitioning at a certain temperature and finish beyond 2–6 °C of the starting point, not melting at a specific temperature or even over a narrow range of temperatures. As a result, the time needed to store heat is reduced, and the cell temperature cannot be kept low for

the required amount of time. Due to the aforementioned issues, attempts to apply PCMs in photovoltaic thermal (PVT) systems to increase water outlet temperatures in the application end and extend heat storage past sunset have not been very successful. In order to improve its thermal performance, this research aims to integrate a PCM with PVT. Energy analysis of electrical and thermal systems has been used to examine performance. The PVT-PCM system, according to the results, achieved lower cell temperatures than other systems.

2. Materials and Methods

The organic paraffin wax PCM is used in the current research to propose a novel framework for photovoltaic thermal (PVT) systems that regulate temperature and store heat. Essentially, experiment-based research was conducted in Malaysian weather. The working principles of PVT and PVT-PCM systems are shown in Figure 1a.

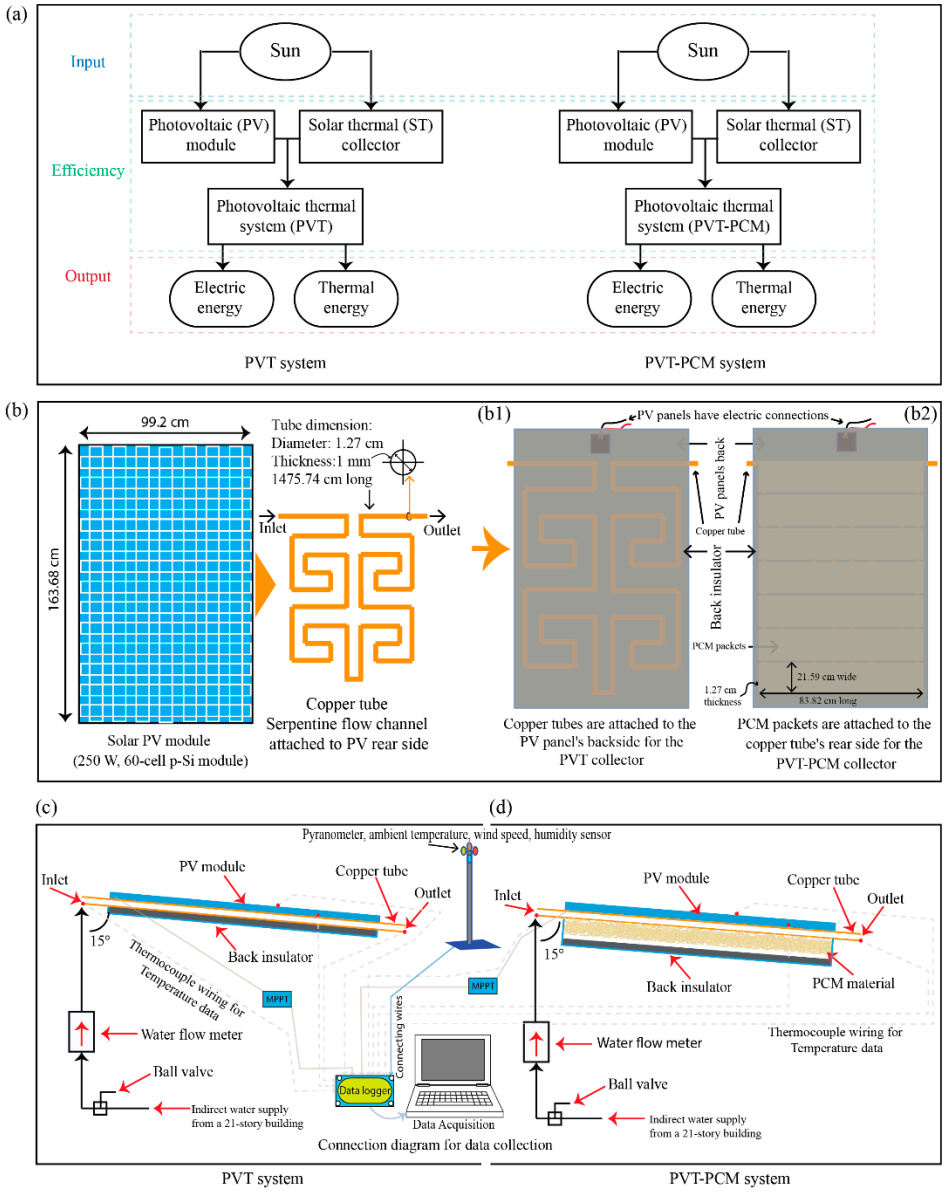

Figure 1. (**a**) Working principle of PVT and PVT-PCM systems; (**b**) PV module, double serpentine flow channel attached to PV rear side; (**b1**) PVT and (**b2**) PVT-PCM thermal collectors; (**c**,**d**) PVT and PVT-PCM experimental setups for onsite comparative performance study.

2.1. PCM Selection

PCM selection for PVT applications depends on the ambient temperature where the module is installed. In Kuala Lumpur, Malaysia, where the average daytime temperature is 33 °C [33], a temperature allowance of 10 to 15 °C is thought to be adequate to capture the majority of the heat from the module. Therefore, PCMs with melting points between 42 and 50 °C can be chosen for the application at hand. In general, organic or inorganic PCMs are better at storing heat in this temperature range.

Any materials that will be used as the PCM in TES systems must have high latent heat and high thermal conductivity. In other words, they must have a melting or freezing temperature that is within the practical range of operation, or at least congruently within a minimum sub-cooling temperature. They also need to be chemically stable, reasonably priced, non-toxic, and non-corrosive. Lauric acid was chosen for the experiment out of the four PCMs that were taken into consideration for this study. The four melting ranges of PCMs and DSC (differential scanning calorimetry) test properties are shown in Table 1. However, the DSC test results are shown in Appendix A.

Table 1. Properties of PCMs.

Name of PCM	Melting Temperature Range (°C)	DSC Test	
Paraffin	52–54	Integral = −1147.47 mJ Normalized = −167.26 Jg^{-1} Onset = 44.70 °C Peak = 52.06 °C Endset = 54.40 °C	x
Lauric acid	44–46	Integral = −711.87 mJ Normalized = 228.90 Jg^{-1} Onset = 42.84 °C Peak = 43.72 °C Endset = 45.76 °C	✓
1-tetradecanol	36–40	Integral = −1608.53 mJ Normalized = −259.44 Jg^{-1} Onset = 36.39 °C Peak = 38.23 °C Endset = 41.28 °C	x
Decanoic acid natural	29–33	Integral = −1591.10 mJ Normalized = −178.98 Jg^{-1} Onset = 30.24 °C Peak = 32.06 °C Endset = 34.97 °C	x

2.2. Fabrication of PVT and PVT-PCM System

The PVT collector has two primary parts: the photovoltaic cell (PV) for generating electricity and the thermal collector (T) for exchanging heat. For the PV device, a 250-Watt 60-cell p-Si module was chosen, which was provided by UMPEDAC. The module's detailed specifications can be found in Table 2.

Table 2. Specification of PV module.

EPV (ENDSUPV Industries)	
Model	**EC61215 (2nd Edition)**
Short Circuit Current: Isc (A)	8.92
Open Circuit Voltage: Voc (V)	38.19
Maximum Power: Pmax (W)	257.59
Current at Pmax: Im (A)	8.41
Voltage at Pmax: Vm (V)	30.60

Note: The electrical characteristics are within 0–3% of the indicated values under Standard Test Conditions (1000 W/m^2, 25 °C. AM 1.5).

For the thermal collector (T), we used thermal absorbers such as copper pipe, water, and PCMs. Materials such as copper pipes are widely used because of their high thermal conductivity. Pipes measure 1.27 cm in diameter, 1 mm in thickness, and 1475.74 cm in length. We used this configuration (copper pipe) to fabricate the PVT collector system as shown in Figure 1b,(b1). For the PVT-PCM collector, we used the same configuration as PVT but added only an extra thermal absorber, which is the PCM. For the PCM packet, we used aluminum materials. The PCM packet has a thickness of 0.5 mm and is constructed from a sheet of aluminum. The PCM packet is wrapped in high-thermal-conductivity, non-adhesive paper, making the packet 1.27 cm thick, 21.59 cm wide, and 83.82 cm long. To fill these PCM packets, we used 8.72 kg of PCM. The full PVT-PCM system is assembled as shown in Figure 1(b2).

2.3. Installation and Instrumentation of the Experimental Setup

After the material selection, preparation, and fabrication, the present PVT and PVT-PCM collectors were installed in the University of Malaya's (UM) Power Energy Dedicated Advanced Centre (UM-PEDAC), in Kuala Lumpur, Malaysia, in its solar garden. Located at 3.1169° N and 101.6669° E [34], this integrated outdoor solar research facility experiences hot weather that is primarily determined by three factors: wind pattern, rainfall, and temperature. However, before the installation of the collectors, there is a need to calculate the panel slope or angle. It is significant because a proper collector slope can allow for more solar radiation. The collector slope is calculated by Cooper's equation (Equation (1)). The slope of the experimental collectors was kept at 15° by combining Equations (1) and (2) [35,36].

The experimental setup is composed of PVT and PVT-PCM, as shown in Figure 1c,d. The configuration was created to investigate the influence of one or more independent variables on the actions of a number of dependent variables. The instrumentation is set in accordance with the need to measure the dependent variables, and the control mechanisms are created to regulate the independent variables. In the current study, electrical and thermal energy are the dependent variables, while inlet flow velocity, incident solar irradiance, water inlet temperature, as well as the temperature of the surrounding air are the independent variables.

2.4. Instrumentation and Data Collection

The connection configuration of different instruments for experimental data collection is shown in Figure 1c,d. Eight thermocouples (K-type [37], RS pro) sensors were used to measure the inlet and outlet water temperatures, as well as the top and back temperatures of the panels. Two manual water flow meters (LZT M-6 [38]) were used to control the flow of water. The data were collected with different water flow rates ranging from 1 to 4 LPM (litres/min). However, the water flow meter was chosen based on tube diameter [39]. In this experiment, indirect water was provided by a supply from a 21-story building at UMPEDAC. A silicon pyranometer (LI-COR, PY82186 [40]) together with an ambient temperature sensor was set up for measuring solar radiation data. Data on wind speed and humidity were collected from a weather station device that was set up at the UMPEDAC solar garden. The electrical parameters (such as open-circuit voltage, Voc; short-circuit current, Isc; maximum voltage, Vm; maximum current, Im; maximum power, Pmax; and fill factor, FF) of the PVT and PVT-PCM modules, on the other hand, were measured and recorded using an I-V tracer (NASA 2.0) with maximum power point tracking (MPPT), as shown in Figure 1c,d, respectively. The I-V tracker, MPPT, and weather station devices were provided by UMPEDAC. A digital data logger (DT80 [41]) was used to continuously record the data. The following Section 2.5.5 provides descriptions of the tools used to measure and record experimental data. Every instrument had been calibrated using standardized techniques.

2.5. Analytical Analysis

2.5.1. Installation of the Modules

Since Malaysia is located in the northern hemisphere of the planet, solar panels have been installed facing south. The slope of the collector (PVT and PVT-PCM), (β) angle of

inclination δ and day of year (d) is calculated from the Equations (1) and (2) of the modules towards the equator [42]:

$$\delta = 23.45 \sin\left[\left(\frac{360}{365}\right)(d + 284)\right] \quad (1)$$

$$\beta = (\varphi - \delta) \quad (2)$$

where δ is the inclination angle (degree),

d is the day of the year (e.g., on January 1, d = 1),
φ is the latitude of the experimental site, and
β is the collector slope (degree).

2.5.2. Estimation of PCM Required

The amount of phase change material essential to absorb the heat produced by a PVT module is estimated by [43–45]. The following Equation (3) can be used to determine the mass of a PCM (m_{PCM}). where the PCM mass (m_{PCM}) is multiplied by the latent heat (L_{PCM}) to melt the PCM [46].

$$m_{PCM} = \frac{Q_{ch}}{L_F + \int_i^m C_{p.s}(T)dT + \int_m^f C_{p.l}(T)dT} \quad (3)$$

where

$C_{p,s}$, $C_{p,l}$ are specific heat of solid and liquid phases of the PCM, respectively;
L_F is the latent heat of PCM;
Q_{ch} is the heat charging phase;
i, m, and f are the initial, melting, and final temperature of PCM;
dT is the temperature rise.

2.5.3. Energy Analysis

The efficiency expressions [47] that combine the thermal efficiency η_{th} and the electrical efficiency η_{el} can be used to represent the performance of PVT and PVT-PCM collectors. These expressions typically include the ratio of the system's useful thermal and electrical gain to the incident solar irradiation on the collector's gap over a given time or period. The system's overall performance is assessed using the total efficiency η_o:

$$\eta_\circ = \eta_{th} + \eta_{el} \quad (4)$$

The thermal performance of the PVT and PVT-PCM units are assessed, and the efficiency parameters are derived using the Hottel–Whillier–Bliss (HWB) [48] modified equations [35,45,49–54]. According to Ibrahim et al. (2014) [55] and Park et al. (2014) [56], the following formulas are used to determine the thermal efficiency (η_{th}) of the conventional flat plate solar collector:

$$\eta_{th} = \frac{\dot{Q}_u}{A \times G} \quad (5)$$

where

Q_u is useful collected heat,
A is the area of the collector, and
G is solar radiation.

Under these conditions, the useful collected heat (Q_u) is given by

$$\dot{Q}_u = \dot{m} C_p (T_{Out} - T_{In}) \quad (6)$$

where

$\dot{m}$ is a mass of water flow rate,
C_p is the is specific heat of water,
T_{Out} is outlet water temperature, and
T_{In} is inlet water temperature.

Equation (7) represents electrical efficiency [45,52,57].

$$\eta_{el} = \frac{P_{\max}}{A \times G} \tag{7}$$

The electrical power output of a PV is

$$P_{el} = I \times V \tag{8}$$

However, the maximum output power in Equation (8) can be a derivative of Equation (9).

$$P_{\max} = I_{sc} \times V_{oc} \times FF = V_{mp} \times I_{mp} \tag{9}$$

The solar energy is converted into electrical and thermal energy by the PVT modules, but the thermal energy is lost through convection, conduction, and radiation.

2.5.4. PV Cell Temperature

The solar cell temperature can be calculated using Equation (10) [58,59]:

$$T_{cell} = \frac{P_{sg} G(\tau_g \alpha - \eta_{el}) + (h_{conv} T_a + h_{rad} T_b)}{h_{conv} + h_{rad}} \tag{10}$$

where

P_{sg} is the packing factor of the solar module;
T_a is the ambient temperature;
T_b is the rear panel temperature;
τ_g is the transmittance of glass;
α is the absorptance;

h_{conv} is the convective heat transfer coefficient as representing by Equation (11) [59]:

$$h_{conv} = 2.8 + 3.v \tag{11}$$

h_{rad} is the radiative heat transfer coefficient between the PVT array and surroundings can be written in Equation (12) [55]:

$$h_{rad} = 1.78 \quad (T_m - T_a) \tag{12}$$

where

v is the wind velocity;
T_m is the panel's top temperature.

The analytical parameters of the solar PVT and PVT-PCM systems are presented in Table 3.

Table 3. Characteristics of the PVT and PVT-PCM systems.

Description	Symbol	Value	Unit
Collector area	A	1.64	m^2
Emittance of glass	εg	0.88	
Emittance of glass plate	εp	0.95	
Collector tilt	β	15	°
Specific heat of the working fluid	C_p	4185.5	J/kg °C
Transmittance of glass	τ_g	0.96	
Absorptance	α	0.90	
Packing factor of the solar module	P_{sg}	0.8	
Initial temperature	i	42.48	°C
Melting temperature	m	43.72	°C
Final temperature	f	45.76	°C
Latent heat	L_F	228.9	KJ/kg

2.5.5. Uncertainty Analysis

An uncertainty analysis of the PVT and PVT-PCM electrical and thermal parameters is performed. The total uncertainty du of a parameter u is composed of the uncertainty of repetition error (du_r) and the uncertainty from equipment error (du_e) [60,61].

$$\delta u = \sqrt{(\delta u_{rep})^2 + (\delta u_{eqp})^2} \tag{13}$$

If U is defined as a function of n independent linear parameters with the formula $U = U\ (u_1, u_2, u_3, \ldots u_m)$ and the parameters $u_1, u_2, u_3, \ldots u_m, u_{m+1} \ldots u_n$ are measured with uncertainties $\delta u_1, \delta u_2, \delta u_3, \ldots, \delta u_m, \delta u_{m+1}, \ldots \delta u_n$ where $U = \frac{u_1 \times u_2 \times u_3, \ldots \times u_m}{u_{m+1} \times \ldots \times u_n}$, then the uncertainty of U will be Equation (14): [61,62]

$$\delta U = \sqrt{\left(\frac{\partial U}{\partial u_1}\delta u_1\right)^2 + \left(\frac{\partial U}{\partial u_2}\delta u_2\right)^2 + \left(\frac{\partial U}{\partial u_3}\delta u_3\right)^2 + \ldots + \left(\frac{\partial U}{\partial u_n}\delta u_n\right)^2} \tag{14}$$

where

dU is the uncertainty of the function U;

du_i is the uncertainty of u_i and $\frac{\partial U}{\partial u_1}$ is the partial derivative of U with respect to u_i.

Therefore, fractional uncertainty of U (assuming that uncertainties in $u_1, u_2, u_3, \ldots u_m, u_{m+1} \ldots u_n$ are separate from one another) will be as follows: [61,63]

$$\frac{\delta U}{U} = \sqrt{\left(\frac{\delta u_1}{u_1}\right)^2 + \left(\frac{\delta u_2}{u_2}\right)^2 + \left(\frac{\delta u_3}{u_3}\right)^2 + \ldots + \left(\frac{\delta u_m}{u_m}\right)^2 + \left(-\frac{\delta u_{m+1}}{u_{m+1}}\right)^2 + \left(-\frac{\delta u_n}{u_n}\right)^2} \tag{15}$$

Fractional uncertainties from energy perspectives can be estimated by using Equation (15) and recalling the energy efficiency equations.

Using the analysis described above, the maximum absolute uncertainty for all parameters is determined to be less than 5% in all experiments. Values of uncertainty inside of this range demonstrate the accuracy of the measured data [60]. Table 4 lists the model, measurement range, and uncertainty information for the various sensors and tools used in the experimental setup.

2.5.6. Economic Analysis

The economic analysis will figure out the payback period of the system. Generally, the payback period is calculated using a standard method. In this study, the annual worth method was established to calculate the system payback period by comparing an initial known system investment with an estimated future operation cost.

The annual worth (*A.W.*) method is the difference between an annual benefit (revenue) and an annual cost [64,65]. Equation (16) shows the basic structure of this method.

$$A.W. = B_A - C_A \tag{16}$$

where

B_A is the annual benefit;
C_A is the annual cost.

Table 4. The instruments' measuring ranges and their associated uncertainties.

Name	Model	Range	Maximum Uncertaintyin Measurement
Pyranometer	LI-COR, PY82186	0 to 2000 W/m^2	±3%
Flow meter	LZT M-6	0.5 to 4.0 L/min	±0.5%
Weather station anemometer and humidity (UMPEDAC)	TM816	0.3 to 30 m/s	±5%
	Testo 608-H1	0 to 50 °C	±0.5%
Thermocouple (type K)	RS pro	−200 to 1000 °C	±0.5%
Data logger	Data Taker DT80	−270 to 1372 °C	±2%
I–V tracer with MPPT (UMPEDAC)	NASA 2.0	50 V 16 A	±4.5%

As a decision-making tool, for acceptance of an option, this expression becomes [66] as follows:

$$B_A - C_A \geq 0 \tag{17}$$

where

$C_1 = C_2 = C_3 = C_N = C_A$ are options for selection if B_A-C_A equals or exceeds zero.

To represent economic analysis between two known systems (such as the PVT and PVT_PCM systems), a cash flow formula could be utilized by this Equation (18). After that, the system needs to be compared to a known system, such as an electric heater, to figure out how long it will take to pay for itself. This is because the whole system is based on heating and cooling performance. Equation (19) shows the cash flow formula for an electric heater system.

$$A.W._{solarsystems} = -(I_c + I_{lc})(A/P, i, N) - A_{rc} - (C_{afic})(A/F, i, N) \tag{18}$$

$$A.W._{electricsystems} = -(I_c + I_{lc})(A/P, i, N) - (R_c) - (H_{erc})(A/F, i, 0.5N) \tag{19}$$

where

I_c is the initial cost;
I_{lc} is the installation cost;
A/P is the capital recovery factor;
i is the interest rate;
N is the life span;
A_{rc} is the annual running cost;
C_{afic} is the repairing cost;
R_c is the running cost;
H_{erc} is the heating element replacement cost.

Any lump-sum payments or benefits must be converted into equivalent uniform periodic time using the capital recovery factors (A/P, i, N) and (A/F, i, N) to use the formula of Equations (20) and (21).

$$A/P = \frac{i(1+i)^N}{(1+i)^N - 1} \tag{20}$$

$$A/F = \frac{i}{(1+i)^N - 1} \tag{21}$$

2.5.7. Market Analysis

A market survey of system cost, initial cost, and operational costs is important for economic analysis. Based on a Malaysian market survey, the PVT, PVT-PCM, and electric

heater system costs have been listed (Appendix B, Tables A1–A3). Renewable energy products, as we all know, are expensive, but their operating periods are much longer than those of non-renewable energy sources [53]. Consequently, this study compares solar energy systems with electric heater systems in order to determine the payback period. Using solar energy to heat water has long-term advantages such as avoiding fuel shortages and helping the environment. The annual worth method is used to calculate the monetary value of the potential savings of using a solar heater as opposed to an electric one. A cash flow chart is used to display the results of the cost analysis.

3. Results and Discussion

The outcomes for PVT and PVT-PCM systems are presented in this section. For PVT and PVT-PCM systems, the daily variation of various parameters with respect to time, including temperatures at various states of points and solar radiation, has been presented.

3.1. Daily Variation of PVT Different Parameters

Figures 2 and 3 show the daily variation of solar radiation and various parameters, including ambient temperature (T_a), water outlet (T_{out}) and inlet (T_{in}) temperature difference (T_{out}-T_{in}), cell temperature (T_{cell}), PV rear side (T_b) temperature, and solar radiation (G), among others. Appendix C contains data on wind speed and humidity for specific days. From May to July 2016, a performance study on the PVT system was conducted. Significant results were attained with the mass flow rates measured at 1, 2, 3, and 4 LPM, respectively. This is an outdoor experiment, so the data depend on Malaysian weather conditions, flow rates, changing materials, and so on. We have recorded and managed a huge data bank. To this end, only the best performance results were studied here based on minimum (1 LPM) and maximum (4 LPM) water flow rates.

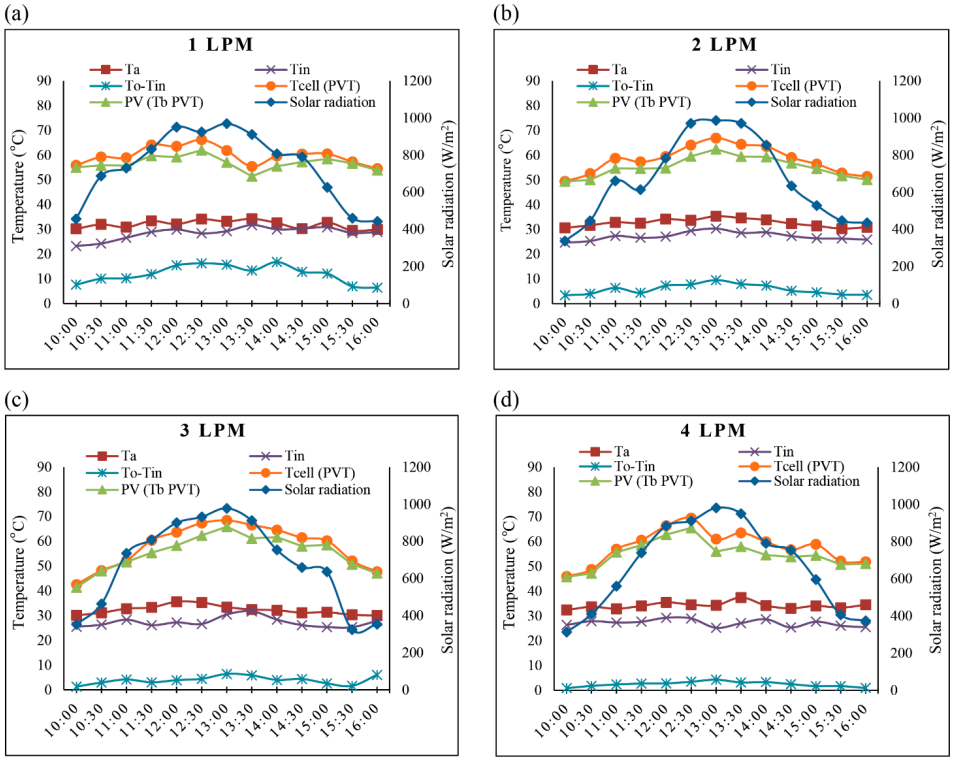

Figure 2. Daily variation of PVT parameters at (**a**) 1 LPM, (**b**) 2 LPM, (**c**) 3 LPM, and (**d**) 4 LPM mass flow rate.

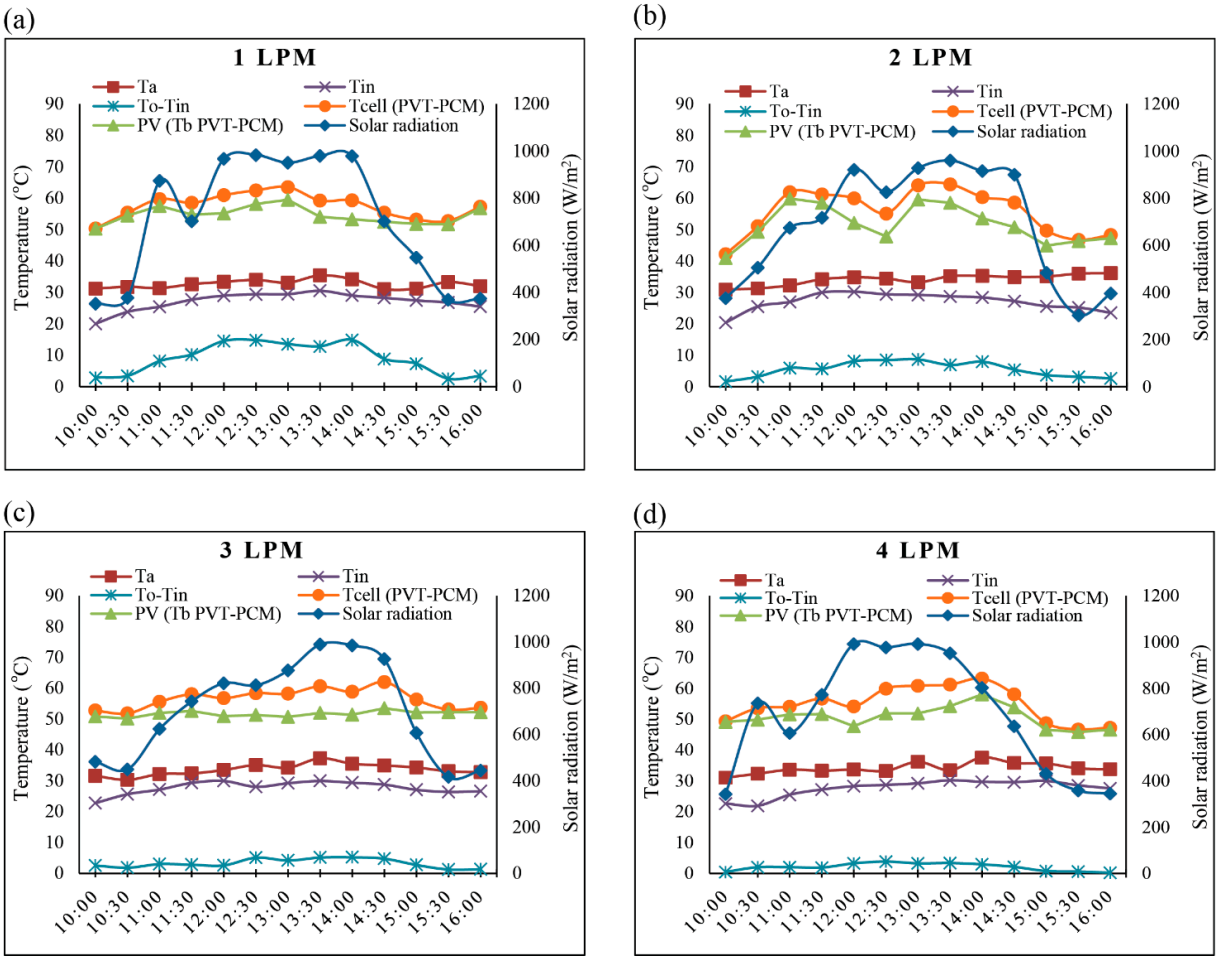

Figure 3. Daily variation of PVT-PCM parameters at (**a**) 1 LPM, (**b**) 2 LPM, (**c**) 3 LPM, and (**d**) 4 LPM flow rate.

Figure 2a shows the variation of solar radiation and temperature in different states of the point PVT system for 1 LPM on 30 May 2016. As can be seen from Figure 2a, the peak solar radiation was 970.21 W/m^2 at 1:00 P.M., and the PVT cell and back temperature difference was found to be 4.75 °C. On that day, the average wind speed, ambient temperature, and humidity were recorded at 3.19 m/s, 31.97 °C, and 52%, respectively. The maximum inlet and outlet water temperature difference was found to be 16.81 °C at 2:00 P.M.

Figure 2b shows that the peak solar radiation was 987.47 W/m^2 at 1:00 P.M., and the PVT cell and back temperature difference was found to be 4.49 °C. On 12 June 2016, the average wind speed, ambient temperature, and humidity were recorded as 1.98 m/s, 32.65 °C, and 75%, respectively. The maximum inlet and outlet water temperature difference was found to be 9.54 °C at 1:00 P.M. at 2 LPM.

Figure 2c, the peak solar radiation was 978.77 W/m^2 at 1:00 P.M., and the PVT cell and back temperature difference was found to be 2.55 °C. On 28 June 2016, the average wind speed, ambient temperature, and humidity were recorded as 2.81 m/s, 32.30 °C, and 63%, respectively. The maximum inlet and outlet water temperature difference was found to be 6.43 °C at 1:00 P.M. at 3 LPM.

On 13 July 2016, the average wind speed, ambient temperature, and humidity were recorded as 1.79 m/s, 34.13 °C, and 63%, respectively. Figure 2d shows that the solar radiation has been rising from 313.18 W/m^2 at 10:00 AM. to a peak value of 980.83 W/m^2 at 1 P.M., which then decreases to 374.01 W/m^2 at 4:00 P.M. Although the solar radiation curve shows a number of unusually sharp declines, it may be concluded that solar radiation peaks between 12:00 and 2:00 P.M. The maximum PVT cell and back temperature difference

was found to be 5.55 °C. Figure 2a also shows that the increase in water temperature is directly correlated with the daily variation in solar radiation, with an increasing trend in the morning, a peak increase at noon, and then a declining trend. At 1 P.M., 4.31 °C is found to be the maximum difference between the inlet and outlet water temperatures at a maximum flow rate of 4 LPM. It is observed that the temperature difference between the cell and the back is highest at this flow rate; cooling is most efficient at 4 LPM as compared to 1, 2, and 3 LPM. This is because a higher mass flow rate results in a more consistent water flow, which more efficiently removes heat from the collector.

Similarly, PVT-PCM systems were installed, and data were collected in August and September of 2016. Figure 3a shows the daily variation of solar radiation and temperatures at various state points of PVT-PCM for a 1 LPM water flow rate on 10 September 2016. At 2 P.M., the highest difference between inlet and outlet water temperatures was 14.87 °C, while the average wind speed, ambient temperature, and humidity remained at 2.43 m/s, 32.68 °C, and 59%, respectively. At 12:30 P.M., the solar radiation peaked at 983.73 W/m^2, while the PVT-PCM cell and back temperature difference measured 4.37 °C.

Figure 3b shows that the peak solar radiation was 960.16 W/m^2 at 1:30 P.M., and the PVT-PCM cell and back temperature difference was found to be 5.88 °C. On 15 September 2016, the average wind speed, ambient temperature, and humidity were recorded as 2.11 m/s, 34.13 °C, and 58%, respectively. The maximum inlet and outlet water temperature difference was found to be 8.66 °C at 1:00 P.M. at 2 LPM.

In Figure 3c, the peak solar radiation was 989.11 W/m^2 at 1:30 P.M., and the PVT-PCM cell and back temperature difference was found to be 8.60 °C. On 18 September 2016, the average wind speed, ambient temperature, and humidity were recorded as 4.34 m/s, 33.63 °C, and 63%, respectively. The maximum inlet and outlet water temperature difference was found to be 5.22 °C at 2:00 P.M. at 3 LPM.

On 20 September 2016, with an average wind speed, ambient temperature, and humidity of 3.64 m/s, 34.17 °C, and 63%, respectively, Figure 3d shows that the daily variation of solar radiation increased from 342.94 W/m^2 at 10:00 A.M. to a peak of 992.23 W/m^2 at 1:00 P.M. and then decreased to 345.12 W/m^2 at 4:00 P.M. The maximum PVT-PCM cell and back temperature difference was found to be 8.97 °C at 12.30 P.M. Between 12:00 and 1:30 P.M., the solar radiation reaches and maintains its peak. The maximum increase in outlet water temperature is 3.86 °C at 12:30 P.M. at 4 LPM. From a comparative standpoint, Figures 2d and 3d show that the PVT-PCM system offers a greater drop in cell temperature than a PVT-only system. The maximum cell temperature drops by 8.97 °C, compared to a maximum drop in cell temperature of about 5.55 °C with a PVT-only system. The phase change material and thermal collector are the two heat transfer media used in the PVT-PCM collector. The PCM receives heat from the collector after it has first been transferred to the water. A huge amount of thermal energy is absorbed by the PCM [51], and once it has properly melted, that thermal energy is again transferred to the water. These procedures improve both the thermal and electrical performance of the cell while also lowering its temperature.

3.2. Electrical Energy Analyses of PVT and PVT-PCM Systems

The energy analysis, which is based on the first law of thermodynamics, provides a generalized picture of how the input energy has been utilized and highlights the key industries that are responsible for the majority of energy consumption. The change in various energy parameters, such as electrical power output, thermal efficiency, electrical efficiency, etc., as a function of solar irradiation, cell temperature, and water flow rate, have been analyzed in the current study to determine which of them has the most pronounced impact on the energy performance of the PVT and PVT-PCM systems. It should be noted that an experimental study on PVT and PVT-PCM was conducted for four different water flow rates to obtain the best electrical performance because the experiment not only studies photovoltaics but also depends on the thermal absorber, PCM, and water flows.

Figures 2a, 3a, 4a and 5a show the solar radiation level, electrical power, and efficiency at a mass flow rate of 1 LPM. The peak solar radiation attained is 970.21 W/m^2, at which the

electrical power of the PVT module is 139.51 W as shown in Figures 2a and 4a, respectively. On the contrary, the PVT-PCM module power output at 983.73 W/m^2 is 143.92 W, as shown in Figures 3a and 5a, respectively. It can be observed that the maximum electrical efficiency of the PVT system is 12.33% at 4:00 P.M., whereas that of the PVT-PCM is 14.25% at 3:30 P.M. as shown in Figures 4a and 5a, respectively.

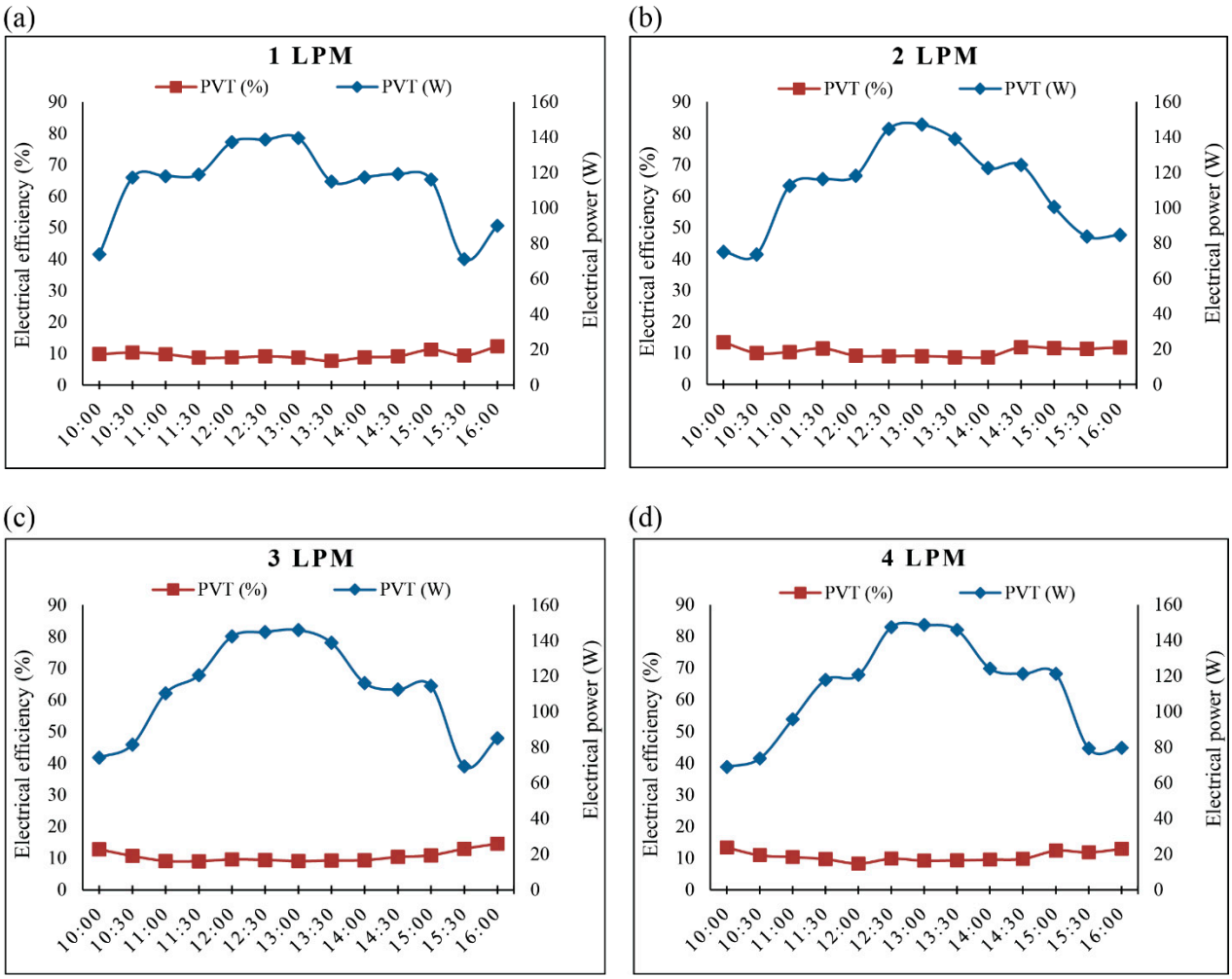

Figure 4. Electrical performance of PVT system at (**a**) 1 LPM, (**b**) 2 LPM, (**c**) 3 LPM, and (**d**) 4 LPM flow rate.

Figures 2b, 3b, 4b and 5b show the solar radiation level, electrical power, and efficiency at a mass flow rate of 2 LPM. The peak solar radiation attained is 987.47 W/m^2, at which the electrical power of the PVT module is 147.25 W, as seen respectively in Figures 2b and 4b. On the contrary, the PVT-PCM module power output at 983.73 W/m^2 is 150.14 W, as shown in Figures 3b and 5b, respectively. It can be observed that the maximum electrical efficiency of the PVT system is 13.48% at 10 A.M., whereas that of the PVT-PCM is 14.11% at 3:00 P.M., as shown in Figures 4b and 5b.

Figures 2c, 3c, 4c and 5c show the solar radiation level, electrical power, and efficiency at a mass flow rate of 3 LPM. The peak solar radiation attained is 978.77 W/m^2, at which the electrical power of the PVT module is 145.92 W as seen in Figures 2c and 4c, respectively. On the contrary, Figures 3c and 5c respectively show that the PVT-PCM module power output at 989.11 W/m^2 is 155.16 W. It can be observed that the maximum electrical efficiency of the PVT system is 14.57% at 4:00 P.M., whereas that of the PVT-PCM is 14.82% at 3:30 P.M., as shown in Figures 4c and 5c respectively.

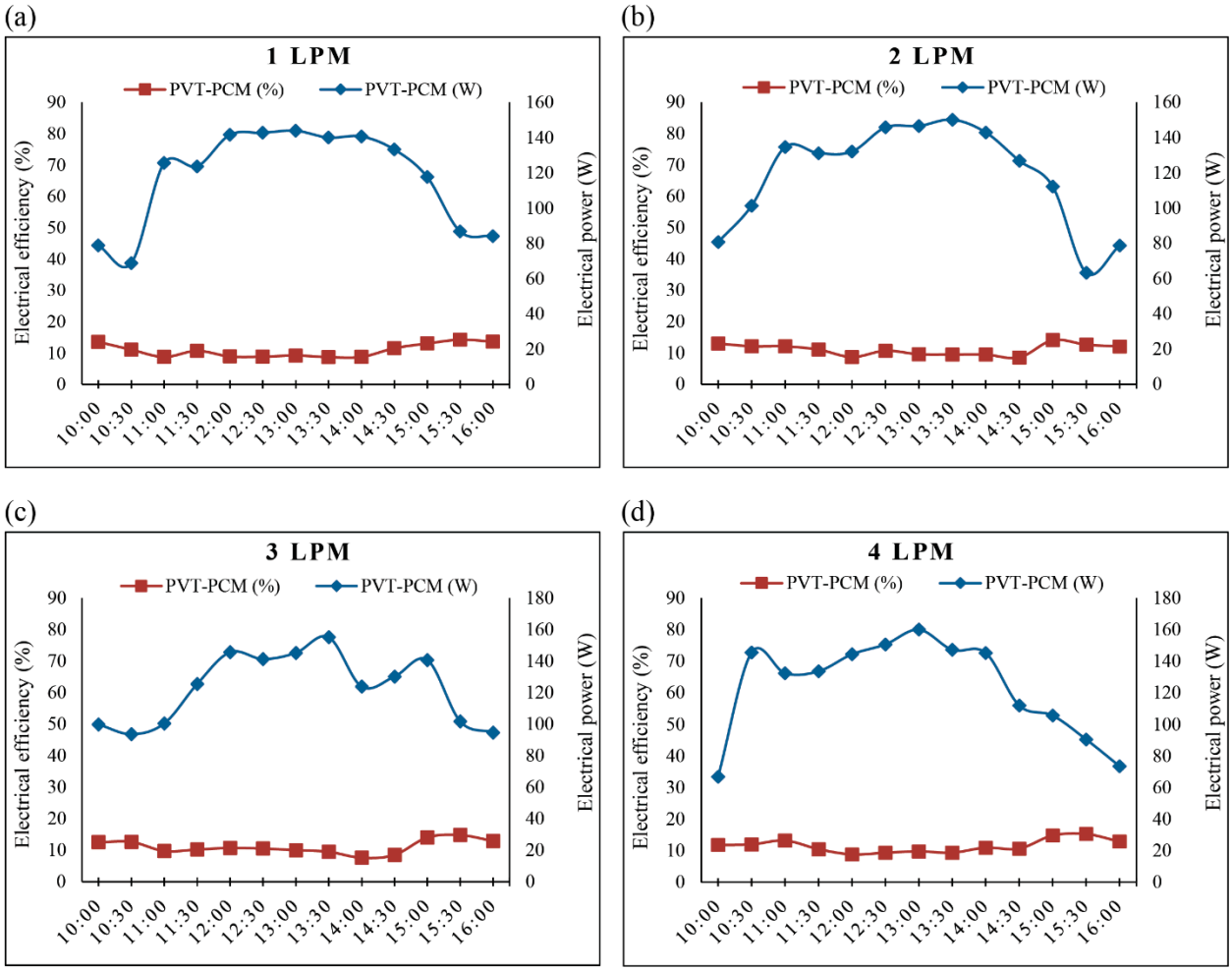

Figure 5. Electrical performance of PVT-PCM system at (**a**) 1 LPM, (**b**) 2 LPM, (**c**) 3 LPM, and (**d**) 4 LPM flow rate.

Figures 2d, 3d, 4d and 5d show how increased irradiation levels affect electrical power and electrical efficiency at a maximum mass flow rate (4 LPM). Figures 2d, 3d, 4d and 5d show that increasing irradiation levels result in an increase in the electrical power and efficiency of PVT and PVT-PCM systems. In both instances, it outperforms the PV modules' power output over the full spectrum of irradiation. These figures highlight a few noteworthy details. The expanding difference between the trend lines of PVT and PVT-PCM systems, as shown in Figures 4d and 5d, illustrates how the cooling effect becomes effective at higher irradiations. At low radiation levels, the difference in temperature between the inlet water and the outlet water is very negligible. The temperature difference grows as the irradiation level rises, mobilizing the rate of heat transfer and assisting in the removal of more heat from the higher irradiations. This tendency is noticeable and more pronounced in the PVT-PCM system, clearly demonstrating the usefulness of the PCM for temperature control.

Secondly, the effect of increased irradiation is no longer as strong after the power output increases at a steeper rate between 300 and 1000 W/m^2. Thus, it can be deduced that, under typical Malaysian weather conditions, irradiation of about 1000 W/m^2 can yield the highest output from a PVT or PVT-PCM panel. Thirdly, Figure 5d shows that the electrical power of the PVT-PCM module is 160.05 W at 992.23 W/m^2, as opposed to 148.61 W at 980.83 W/m^2 for the PVT module, as shown in Figure 4d, clearly demonstrating an increase in the power output when the PCM and mass flow rate are used for thermal control. Results indicate that different levels of illumination cause solar cells to produce different amount of power. With a relatively small increase in panel voltage, the panel

current rises in direct proportion to solar radiation. Similarly, to this, panel power rises in proportion to the amount of solar radiation.

According to Figures 4d and 5d, at 1 P.M., the maximum output powers of PVT-PCM and PVT differ by 11.44 W. The ability of phase change materials to store a large amount of heat allows the cell temperature to be kept as close to the STC value as possible, improving electrical output. Figures 4d and 5d show the response of electrical efficiency as a function of the irradiation of PVT and PVT-PCM modules, respectively. The data clearly show that the efficiency of both PVT and PVT-PCM photovoltaic devices increases up to an irradiation level of about 300 to 600 W/m^2 and then noticeably decreases with increased irradiation. Therefore, in Malaysian conditions, photovoltaic devices function best within the aforementioned range of irradiation. Consequently, the PV/T-PCM module produces a commendably superior performance to the PV/T-only system operating alone. Figure 4d illustrates that the electrical efficiency of the PVT module decreases from 13.36% to 8.28% as the irradiation level rises from 313.18 to 883.77 W/m^2.

On the other hand, as seen in Figure 5d, the electrical efficiency of the PVT-PCM module decreases from 15.32% to 8.83% as the irradiation level rises from 358.45 to 991.85 W/m^2. The electrical efficiencies of PVT and PVT-PCM systems differ by a maximum of 1.96% in Figures 4d and 5d. It can be noticed that the PVT system's maximum electrical efficiency is 13.36% at 10 A.M., as shown in Figure 4d, whereas that of the PVT-PCM system is 15.32% at 3:30 P.M., as shown in Figure 5d, clearly demonstrating a notable improvement in the electrical performance by using PCM. This confirms that using PCM thermal control in PVT systems is the right decision, which holds true not only for the highest efficiency point but also for almost the entire range of efficiency.

3.3. Thermal Energy Analyses of PVT and PVT-PCM Systems

Figure 6 provides information on of the average thermal performance of PVT and PVT-PCM systems. The performance is shown in terms of outlet water temperature, heat gain, and thermal efficiency. Figure 6a presents the heat gain as well as the thermal efficiency of PVT and PVT-PM modules, respectively. While PVT and PVT-PCM collectors are designed to produce both electricity and heat, one of their main uses is in the provision of warm water. In this case, the temperature of the water coming out of the collector has been used as an indicator of its thermal performance, along with the amount of heat it gains and how well it uses that heat.

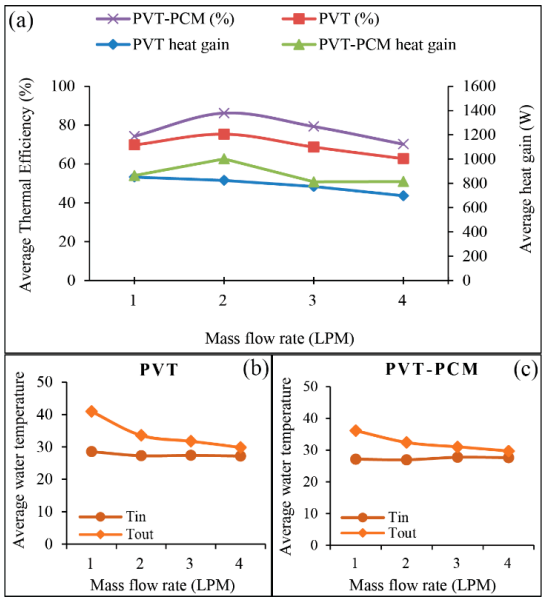

Figure 6. (**a**) Average thermal efficiency, heat gain, and (**b**,**c**) water temperature of PVT and PVT-PCM collectors as a function of water flow rate.

The inlet and outlet water temperatures generated by the PVT and PVT-PCM systems are depicted in Figure 6b,c, respectively. Both graphs clearly show that as the water flow rate increases, the temperature of the outlet water decreases. Therefore, the flow rate may be kept at 2 LPM to obtain a warm water supply with better thermal efficiency. For PVT systems, the maximum average heat gain is 851.91 W at 1 LPM, and the highest obtainable thermal efficiency is 75.29% at 2 LPM. On the other hand, PVT-PCM modules offer the highest average thermal efficiency at 86.19% with a heat gain of 1001.71 W at 2 LPM. So, the use of PCMs makes it easy to obtain 149.80 W more heat output and 10.90% more thermal efficiency than with a traditional PVT system.

4. Comparative Performance Evaluation

This study also compares the performance of two systems, PVT and PVT-PCM, as well as another existing study so that it can understand the use of PCMs with different mass flow rates of water. Figure 7a,b show the average electrical and thermal efficiencies of PVT and PVT-PCM with different water flow rates. It is observed that both the electrical and thermal performance of the PVT-PCM is better than that of the PVT system. While the maximum PVT panel electrical efficiency obtained is 10.56% (Figure 7a), at 4 LPM of water flow rate, the PVT-PCM system offers almost a 0.95% increase with respect to 11.51% (Figure 7b). The maximum thermal efficiency of the PVT-PCM collector is enhanced by 10.90% at 2 LPM as compared to the PVT collector.

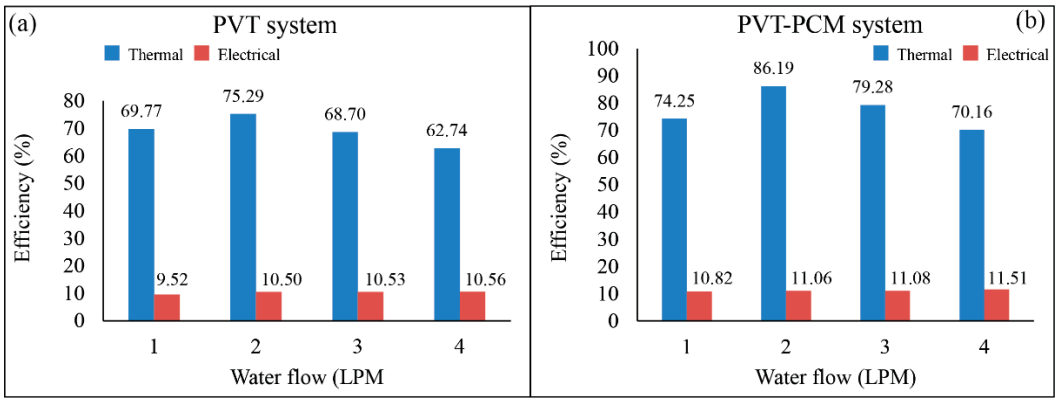

Figure 7. Average energy efficiency comparison performance of (**a**) PVT and (**b**) PVT-PCM for different mass flow rates.

Table 5 compares the performance parameters of PVT and PVT-PCM systems obtained in the current study to those obtained in previous research. It can be seen from the table that these results agree well with the previous ones. However, PVT and PVT-PCM electrical and thermal performance with the proposed system have improved since the previous studies.

Table 5. Comparative performance assessment of the present with the previous study. Reprinted/adapted with permission from Ref. [52], 2023, Elsevier, License number 5491951000896.

Type of Systems	Electrical Efficiency (%)	Thermal Efficiency (%)	Reference
PVT system	9.92	72	[66]
PVT system	10.8	62.37	[67]
PV/T and PV/T-PCM system	6.98 and 8.16	58.35 and 69.84	[68]
PV-TES	×	40 to 50	[69]
NPVT and NPV-TES	1.59 and 3.19	×	[70]
PV/PCM and Reflector/PCM/Nonpractical	12.49 and 12.84	×	[71]
PVT and PVT-PCM	10.56 and 11.51	75.29 and 86.19	(Present)

5. Economic Analysis

The economic analysis focuses on the payback time for the entire system, which consists of the solar system (PVT and PVT-PCM) and the electric heater system. These results help to differentiate between the economic performance of renewable and non-renewable sources. The cash flow diagram and the total cost over 25 years for a solar PVT and PVT-PCM system can be predicted from the assumed years using Equations (18), (20), and (21). The cash flow life expectancy of the module can be determined using the information in Tables A1 and A2 of Appendix B, assuming an annual interest rate of 10%. This calculation is a pragmatic estimate based on some assumed values. In contrast, Appendix D (Figure A5 and Table A5) displays the payback results from the cost analysis of an electric heater using Equations (19)–(21), respectively.

The cost of the thermal absorber is MYR 1750.77 (USD 410.78). Note that the USD conversion rate was 1 US$ = 4.26 MYR. The cash flow diagram of a PVT is depicted in Figure 8 from year 0 to year 25, with values and arrows showing the year and cost per 15-year period of MYR 100 (US$23.46). With zero annual operating costs, as displayed in Table A1, the total outlay is MYR 3750.77 (US$880.09), including MYR 100 (US$23.46) for setup. After 25 years of use, a replacement fee of MYR 100 (US$23.46) is added for each component part that needs to be replaced.

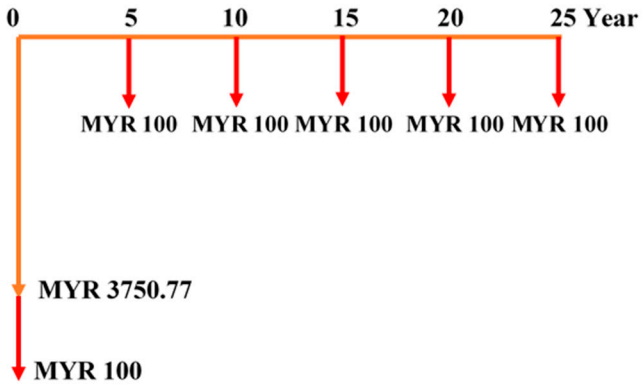

Figure 8. Solar PVT system cash flow diagram.

Cost of running a solar PVT system:
First 5 years:

$$A.W._{solar\ PVT} = \text{MYR} - 1032.20\ (\text{US\$}\ 242.30)$$

Second 10 years:

$$A.W._{solar\ PVT} = \text{MYR} - 632.96\ (\text{US\$}\ 148.58)$$

Third 15 years:

$$A.W._{solar\ PVT} = \text{MYR} - 509.42\ (\text{US\$}\ 119.58)$$

Fourth 20 years:

$$A.W._{solar\ PVT} = \text{MYR} - 454.05\ (\text{US\$}\ 106.58)$$

Fifth 25 years:

The cost of the solar PVT system is represented by the negative values. The cost of the solar PVT system has a longer payback period than the electric heater system, according to the annual worth method, but after 20 years, the cost value is MYR 454.05 (US$106.58), which is less than MYR 492.05 (US$115.50) (electric heater system, Table A5). The payback period for the solar PVT system will start after 20 years, based on the annual worth method.

MYR 1750.77 (US$410.97) is expected for the thermal absorber and MYR 1853.76 (US$435.15) for the PCMs. Figure 9 shows a PCM cash flow diagram from year 0 to year 25, with values and arrows representing the year and MYR 1900 (US$446 per 5-year period). From Table A2, it is stated that zero cost is encountered in the initial year; thus, MYR 5604.53 (US$1315.61) is the initial cost, plus MYR 1900 as the installation cost. While the annual operating cost is zero, PCMs will need to be replaced after 5 years, which will cost MYR 1900 (US$446) in addition to the replacement of some component parts.

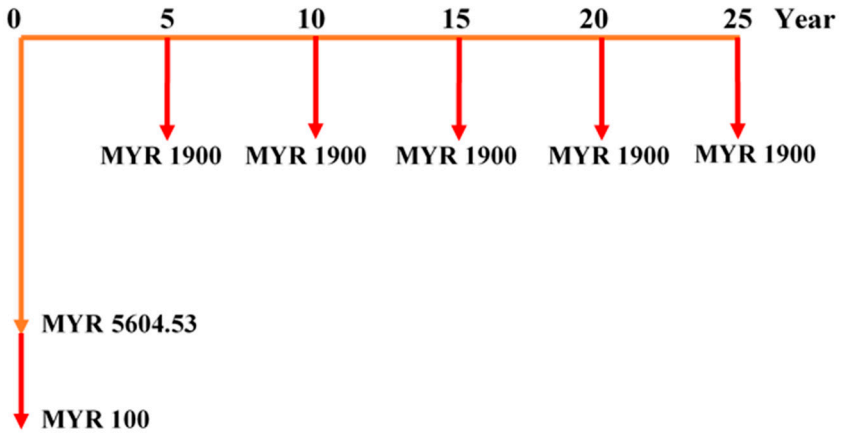

Figure 9. Solar PVT-PCM system cash flow diagram.

Cost of running a solar PVT-PCM system:
First 5 years:

$$A.W._{\ solar\ PVT\text{-}PCM} = \text{MYR} - 1816.05\ (\text{US\$426.30})$$

Second 10 years:

$$A.W._{\ solar\ PVT\text{-}PCM} = \text{MYR} - 1047.60\ (\text{US\$245.91})$$

Third 15 years:

$$A.W._{\ solar\ PVT\text{-}PCM} = \text{MYR} - 809.79\ (\text{US\$190.09})$$

Fourth 20 years:

$$A.W._{\ solar\ PVT\text{-}PCM} = \text{MYR} - 703.22\ (\text{US\$165.05})$$

Fifth 25 years:

Furthermore, MYR 1900 (US$446) as the replacement cost for its parts is expected at the 25-year mark, bringing the total to MYR – 647.77 (US$152.05).

The negative values represent the solar PVT-PCM system's cost values. A solar PVT-PCM system costs significantly more than an electric heater system; even after 25 years, the cost value is MYR 647.77 (US$151.78). This means that the lifetime of PV panels can be increased, allowing them to be used for a longer period of time. Based on the findings, it is clear that the solar PVT-PCM system has a longer service life than the solar PVT system.

6. Conclusions

The objective of this study was to examine and contrast the performance of a PVT and a PVT-PCM module under typical weather conditions in Malaysia. Energy analyses have been performed to evaluate the system's overall performance. The following are the main conclusions:

- The highest PVT and PVT-PCM electrical power outputs of 148.61 W and 160.05 W are attained with a flow rate of 4 LPM, respectively.
- For the PVT and PVT-PCM systems, the maximum electrical efficiencies are 14.57% at 3 LPM and 15.32% at a maximum flow rate of 4 LPM.
- The maximum PVT average thermal efficiency is 75.29% with a mass flow rate of 2 LPM, while the highest rise in the outlet water temperature is 16.81 °C at 1 LPM. The lowest water temperature difference is 4.31 °C at 4 LPM.
- The maximum PVT-PCM average thermal efficiency is 86.19% with a mass flow rate of 2 LPM, while the highest rise obtained is 14.87 °C at 1 LPM. The lowest water temperature difference is 3.86 °C at 4 LPM because of the effect of the extra thermal absorber PCMs.
- The economic analysis shows that the solar PVT system's payback period will start after 20 years compared to an electric heater system. The solar PVT-PCM system, on the other hand, costs significantly more than the solar PVT and electric heater system but has a longer service life than the solar PVT system.

Author Contributions: Conceptualization, M.S.H.; methodology, M.S.H.; software, M.S.H. and L.K.; validation, M.S.H., J.S., A.K.P. and N.A.R.; formal analysis, M.S.H., L.K. and A.A.; investigation, M.S.H.; resources, N.A.R.; data curation, M.S.H.; writing—original draft preparation, M.S.H.; writing—review and editing, M.S.H., A.A. and L.K.; visualization, M.S.H.; supervision, M.S.H., J.S., A.K.P. and N.A.R.; project administration, N.A.R.; funding acquisition, N.A.R. All authors have read and agreed to the published version of the manuscript.

Funding: This research was funded by UM Power Energy Dedicated Advanced Centre (UMPEDAC), University of Malaya.

Institutional Review Board Statement: This information is handled by the University of Malaya Education Authority. Further information could be provided upon request.

Informed Consent Statement: Not applicable.

Data Availability Statement: All data used to support the findings of this study are included in the article. The data presented in this study are available on request.

Conflicts of Interest: The authors declared no potential conflicts of interest with respect to the research, authorship, and/or publication of this article.

Appendix A. PCMs DSC Test Report

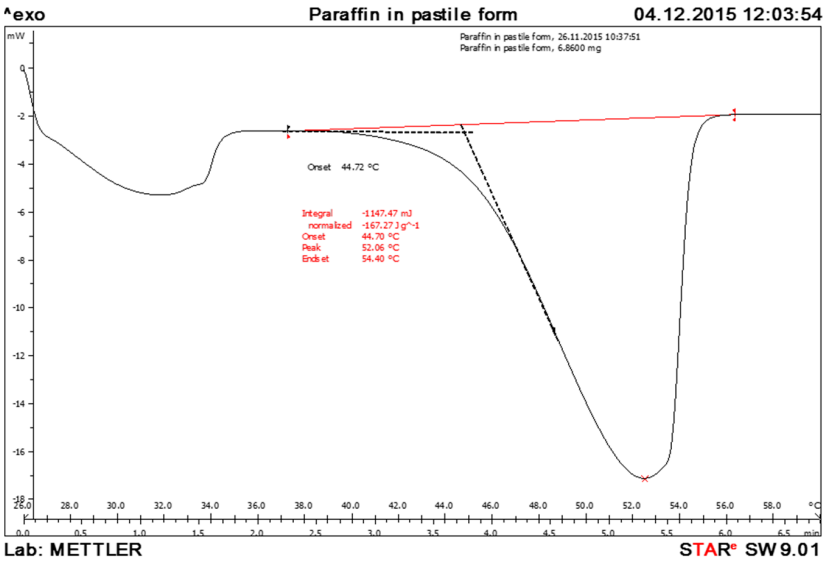

Figure A1. Paraffin DSC test curve.

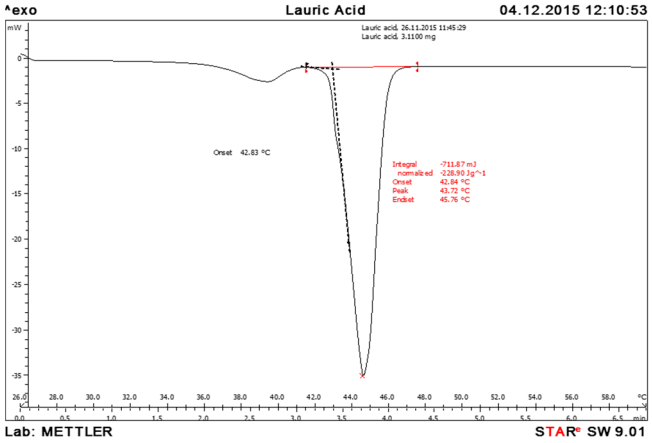

Figure A2. Lauric acid DSC test curve.

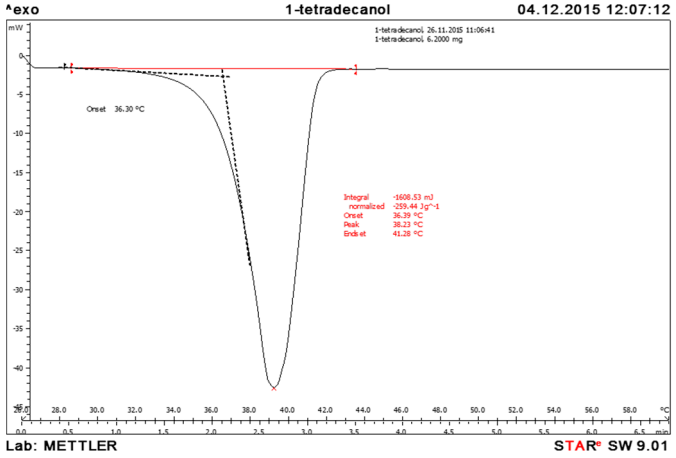

Figure A3. I-tetradecanol DSC test curve.

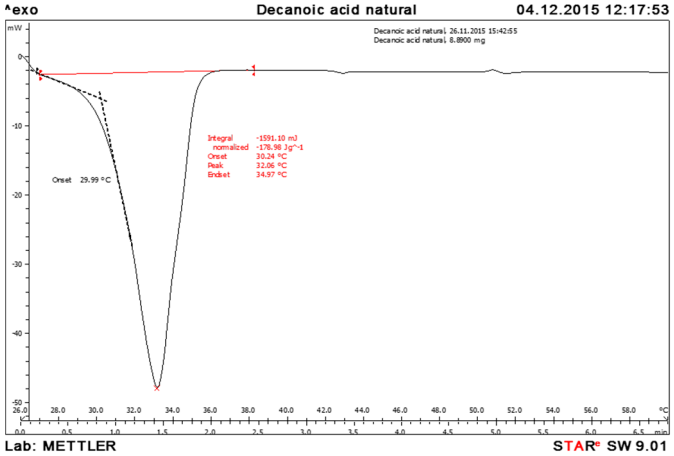

Figure A4. Decanoic acid natural DSC test curve.

Appendix B. PVT and PCM System Cost

Table A1. The breakdown cost of solar PV module and thermal collector (PVT system).

Component	Description	Retail Price (MYR)
Solar PV module cost	60 cells-Poly 250 W	2000
Salvage value		0
Total retail cost		2200 (US$516.43)
Thermal collector	Absorber aluminum sheet (1 mm, 39, 58 inch)	36
	Absorber copper pipe (1 mm, 0.5-inch, 581 inch)	280.77
	Copper pipes elbow connector (0.5-inch dia, 68 pieces)	578
	Pipe to absorber sheet gaps fill up with heat conducting paste	30
	Aluminum foil cover	30
Insulation sheet	Ceramic fiber paper	50
Plywood sheet	6 mm plywood (2.5, 3 fit)	30
Back cover sheet	Aluminum 1mm sheet	36
Inlet, outlet pipe	6 m palate 0.5 m dia	20
Gate valves	Mattel and plastic	30
Storage tank	80-gallon plastic tank	180
Water flow meter	0.5 to 4 water LPM	250
Other	Pudding, screw, rods, silicone paste, etc.	200
Installation cost		100
Salvage value		0
Total retail cost		1750.77 (US$ 410.97)

Table A2. The breakdown cost of PCM.

Component	Description	Retail Price (MYR)
PCM	Phase change material (lauric acid, 8.72 kg)	1813.76
Aluminum packets for PCM	7 packets	40
Installation cost		100
Salvage value		0
Total retail cost		1853.76 (US$ 435.15)

Table A3. Cost of all components for constructing electric heater. Reprinted/adapted with permission from Ref. [45], 2023, Elsevier, License number 5491950164169.

Component	Description	Retail Price (MYR)
Price of electric heater	Electric water heater (DSK-55) 5500 W	386.16
Price of the heating element	Copper	200
Installation cost		100
Running cost		431.46
Total retail cost		686.16 (US$ 160.56)

Appendix C. Wind and Humidity Data

Table A4. Wind and Humidity Data (selected month).

30 May 2016				**12 June 2016**			
Time	**Humidity (%)**	**Wind Direction**	**Wind Speed (m/s)**	**Time**	**Humidity (%)**	**Wind Direction**	**Wind Speed (m/s)**
10:00 A.M.	66	N	0.45	**10:00 A.M.**	84	W	3.13
11:00 A.M.	52	NW	3.13	**11:00 A.M.**	84	WNW	1.34
12:00 P.M.	52	NNW	3.58	**12:00 P.M.**	79	NNE	2.24
1:00 P.M.	49	NNW	3.13	**1:00 P.M.**	70	NW	2.24
2:00 P.M.	47	NW	4.02	**2:00 P.M.**	75	W	1.34
3:00 P.M.	47	NNW	4.02	**3:00 P.M.**	66	NW	1.34
4:00 P.M.	49	WNW	4.02	**4:00 P.M.**	66	N	2.24
28 June 2016				**13 July 2016**			
Time	**Humidity (%)**	**Wind Direction**	**Wind Speed (m/s)**	**Time**	**Humidity (%)**	**Wind Direction**	**Wind Speed (m/s)**
10:00 A.M.	74	SE	3.13	**10:00 A.M.**	79	NE	0.89
11:00 A.M.	70	SSE	3.13	**11:00 A.M.**	70	NE	0.45
12:00 P.M.	66	S	3.13	**12:00 P.M.**	62	SE	0.89
1:00 P.M.	63	S	3.13	**1:00 P.M.**	59	S	4.02
2:00 P.M.	59	SSW	2.24	**2:00 P.M.**	59	S	2.24
3:00 P.M.	56	S	2.24	**3:00 P.M.**	56	WSW	1.34
4:00 P.M.	56	WSW	2.68	**4:00 P.M.**	56	SW	2.68
10 September 2016				**15 September 2016**			
Time	**Humidity (%)**	**Wind direction**	**Wind speed (m/s)**	**Time**	**Humidity (%)**	**Wind direction**	**Wind speed (m/s)**
10:00 A.M.	70	SE	0.89	**10:00 A.M.**	70	S	1.34
11:00 A.M.	62	ESE	2.24	**11:00 A.M.**	66	SSE	1.34
12:00 P.M.	59	E	2.68	**12:00 P.M.**	62	S	2.24
1:00 P.M.	55	SSE	2.24	**1:00 P.M.**	59	WSW	2.24
2:00 P.M.	55	SE	3.13	**2:00 P.M.**	49	S	2.24
3:00 P.M.	56	S	2.68	**3:00 P.M.**	52	WSW	2.24
4:00 P.M.	59	SSW	3.13	**4:00 P.M.**	49	W	3.13
18 September 2016				**20 September 2016**			
Time	**Humidity (%)**	**Wind direction**	**Wind speed (m/s)**	**Time**	**Humidity (%)**	**Wind direction**	**Wind speed (m/s)**
10:00 A.M.	70	NW	3.13	**10:00 A.M.**	70	NNW	4.02
11:00 A.M.	66	NW	4.02	**11:00 A.M.**	66	NW	5.36
12:00 P.M.	62	NNW	3.58	**12:00 P.M.**	62	NNW	3.13
1:00 P.M.	59	NW	5.36	**1:00 P.M.**	59	WNW	3.58
2:00 P.M.	56	WNW	4.02	**2:00 P.M.**	66	SW	3.58
3:00 P.M.	63	W	4.47	**3:00 P.M.**	62	W	3.13
4:00 P.M.	63	W	5.81	**4:00 P.M.**	55	W	2.68

Appendix D. Electric Heater Cash Flow Results

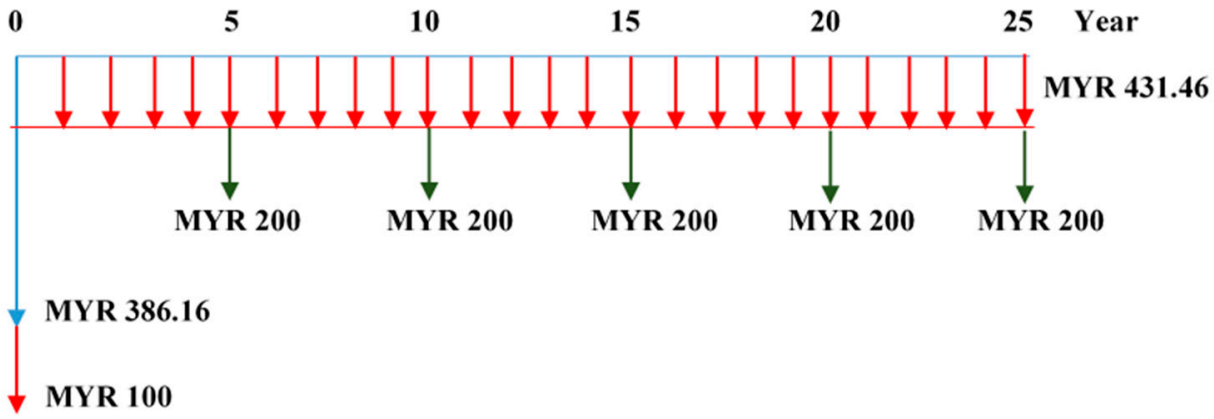

Figure A5. Electric heater cash flow diagram.

Table A5. Cost of running an electrical heater.

Year	A.W. Electric Heater (MYR)	US$
5	592.46	138.05
10	523.12	122.79
15	501.67	117.76
20	492.05	115.50
25	487.05	114.33
30	484.24	113.67

References

1. Victoria, H. The Next Solar Frontier: Hybrid PV/Thermal Systems. *Conserv. Eng.* 2009. Available online: https://www.renewableenergyworld.com/rea/news/article/2009/12/the-next-solar-frontier-producing-more-energy-with-hybrid-pvthermal-systems (accessed on 18 October 2022).
2. Braunstein, A.; Kornfeld, A. On the development of the solar photovoltaic and thermal (PVT) collector. *IEEE Trans. Energy Convers.* **1986**, *EC-1*, 31–33. [CrossRef]
3. Cox, I.C.; Raghuraman, P. Design considerations for flat-plate photovoltaic/ thermal collectors. *Sol. Energy* **1985**, *35*, 227–241. [CrossRef]
4. Lalovic, B. A hybrid amorphous silicon photovoltaic and thermal solar collector. *Sol. Cells* **1986–1987**, *19*, 131–138. [CrossRef]
5. Raghuraman, P. Analytical prediction of liquid and air photovoltaic/thermal flat plate collector performance. *J. Sol. Energy Eng.* **1981**, *103*, 291–298. [CrossRef]
6. Garg, H.P.; Agarwal, R.K.; Joshi, J.C. Experimental study on a hybrid photovoltaicthermal solar water heater and its performance predictions. *Energy Convers. Manag.* **1994**, *35*, 621–633. [CrossRef]
7. Agarwal, R.K.; Garg, H.P. Study of a photovoltaic-thermal system—Thermosyphonic solar water heater combined with solar cells. *Energy Convers. Manag.* **1994**, *35*, 605–620. [CrossRef]
8. Bhargava, A.K.; Garg, H.P.; Agarwal, R.K. Study of a hybrid solar system–solar air heater combined with solar cell. *Sol. Energy* **1991**, *31*, 471–479. [CrossRef]
9. Shouquat, H.M.; Abd, R.N.B.; Selvaraj, J.A.L.; Pandey, A.K. Experimental Investigation on Energy Performance of hybrid PV/T-PCM system. In Proceedings of the 2019 Fifth International Conference on Electrical Energy Systems (ICEES), Chennai, India, 21–22 February 2019; pp. 1–5.
10. de Vries, D. Design of a Photovoltaic/Thermal Combi-Panel. Ph.D. Thesis, Eindhoven Technical University, Eindhoven, The Netherland, 1998.
11. Hossain, S.; Abbas, A.W.; Selvaraj, J.; Ahmed, F.; Abd Rahim, N. Experiment of a Flat Plate Solar Water Heater Collector with Modified Design and Thermal Performance Analysis. *Appl. Mech. Mater.* **2014**, *624*, 332–338. [CrossRef]
12. Florschuetz, L. On heat rejection from terrestrial solar cell arrays with sunlight concentration. In Proceedings of the 11th IEEE PVSC Conference, New York, NY, USA, 9–11 June 1975; pp. 318–326.

13. Florschuetz, L. Extension of the Hottel–Whiller model to the analysis of combined photovoltaic/thermal flat plate collectors. *Sol. Energy* **1979**, *22*, 361–366. [CrossRef]
14. Hendrie, S. Evaluation of combined photovoltaic/thermal collectors. In Proceedings of the ISES International Congress, Atlanta, GA, USA, 28 May–1 June 1979; Volume 3, pp. 1865–1869.
15. Kern, J.; Russell, M. Combined photovoltaic and thermal hybrid collector systems. In Proceedings of the 13th IEEE Photovoltaic Specialists, Washington, DC, USA, 15–19 August 1978; pp. 1153–1157.
16. Wolf, M. Performance analysis of combined heating and photovoltaic power systems for residences. *Energy Convers. Manag.* **1976**, *16*, 79–90. [CrossRef]
17. Kalogirou, S.; Tripanagnostopoulos, Y. Hybrid PV/T solar systems for domestic hot water and electricity production. *Energy Convers. Manag.* **2006**, *47*, 3368–3382. [CrossRef]
18. Chow, T.T. A review on photovoltaic/thermal hybrid solar technology. *Appl. Energy* **2010**, *87*, 365–379. [CrossRef]
19. Hameed Jaaz, A.; Hasan, H.A.; Sopian, K.; Kadhum, A.A.H.; Gaaz, T.S.; Al-Amiery, A.A. Outdoor Performance analysis of a photovoltaic thermal (PVT) collector with Jet impingement and compound parabolic concentrator (CPC). *Materials* **2017**, *10*, 888. [CrossRef]
20. Teo, H.G.; Lee, P.S.; Hawlader, M.N.A. An active cooling system for photovoltaic modules. *Appl. Energy* **2012**, *90*, 309–315. [CrossRef]
21. Lianos, P. Review of recent trends in photoelectrocatalytic conversion of solar energy to electricity and hydrogen. *Appl. Catal. B Environ.* **2017**, *210*, 235–254. [CrossRef]
22. Tyagi, V.V.; Kaushik, S.C.; Tyagi, S.K. Advancement in solar photovoltaic/thermal (PV/T) hybrid collector technology. *Renew. Sustain. Energy Rev.* **2012**, *16*, 1383–1398. [CrossRef]
23. Adham, M.; Sidding, O.; Hisham, S. Advancements in hybrid photovoltaic systems for enhances solar cells performance. *Renew. Sustain. Energy Rev.* **2015**, *41*, 658–684.
24. Sharma, A.; Tyagi, V.V.; Chen, C.R.; Buddhi, D. Review on thermal energy storage with phase change materials and applications. *Renew. Sustain. Energy Rev.* **2009**, *13*, 318–345. [CrossRef]
25. Telkes, M. Thermal energy storage in salt hydrates. *Sol. Energy Mater.* **1980**, *2*, 381–393. [CrossRef]
26. Pielichowska, K.; Pielichowski, K. Phase change materials for thermal energy storage. *Prog. Mater. Sci.* **2014**, *65*, 67–123. [CrossRef]
27. Stultz, J.W. *Thermal and Other Tests of Photovoltaic Modules Performed in Natural Sunlight*; Report number: DOE/JPL/1012-9, Technical Report; Jet Propulsion Laboratory: Pasadena, CA, USA, 1978. [CrossRef]
28. Huang, M.J.; Eames, P.C.; Norton, B. Thermal regulation of building-integrated photovoltaics using phase change materials. *Int. J. Heat Mass Trans.* **2004**, *47*, 2715–2733. [CrossRef]
29. Hasan, A.; McCormack, S.; Huang, M.; Norton, B.J.S.E. Evaluation of phase change materials for thermal regulation enhancement of building integrated photovoltaics. *Sol. Energy* **2010**, *84*, 1601–1612. [CrossRef]
30. Browne, M.C.; Quigley, D.; Hard, H.R.; Gilligan, S.; Ribeiro, N.C.; Almeida, N.; McCormack, S.J. Assessing the thermal performance of phase change material in a photovoltaic/thermal system. *Energy Procedia* **2016**, *91*, 113–121. [CrossRef]
31. Sharma, R.K.; Ganesan, P.; Tyagi, V.V.; Mahlia, T.M.I. Accelerated thermal cycle and chemical stability testing of polyethylene glycol (PEG) 6000 for solar thermal energy storage. *Sol. Energy Mater. Sol. Cells* **2016**, *147*, 235–239. [CrossRef]
32. Pandey, A.K.; Hossain, M.S.; Tyagi, V.V.; Abd Rahim, N.; Selvaraj, J.A.L.; Sari, A. Novel approaches and recent developments on potential applications of phase change materials in solar energy. *Renew. Sustain. Energy Rev.* **2018**, *82*, 281–323. [CrossRef]
33. MetMalaysia. Malaysia meteorology department. *Off. Website* **2020**. Available online: https://www.met.gov.my/forecast/weather/state/ (accessed on 1 May 2016).
34. SunEarthTools, C. Tools for Consumers and Designers of Solar. Software. 2016. Available online: http://www.sunearthtools.com/dp/tools/pos_sun.php (accessed on 3 June 2016).
35. Hossain, M.S. Thermal Performance and Economic Analysis of Solar Photovoltaic Water Heater under the Malaysian Climatic Condition. Master Thesis, Universiti Malaya, Kuala Lumpur, Malaysia, 2013.
36. Struckmann, F. Analysis of a Flat-plate Solar Collector. *Heat Mass Transp. Proj. Rep.* **2008**. Available online: http://www.ht.energy.lth.se/fileadmin/ht/Kurser/MVK160/Project_08/Fabio.pdf (accessed on 5 June 2016).
37. Element14. Thermocouples. 2015. Available online: https://my.element14.com/c/sensors-transducers/sensors/temperature-sensors/thermocouples?thermocouple-type=k (accessed on 17 July 2016).
38. Alibaba.com. lmz15 Panel Type Water Flow Meter lmz15 Panel Mount Water Flow Meter Air Flow Meter lzt-6. 2015. Available online: https://www.alibaba.com/product-detail/lmz15-panel-type-water-flow-meter_62516688234.html?spm=a2700.7724857.0.0.63c74b0fomkRVg (accessed on 18 May 2016).
39. LORRIC. Relationship between Flow Rate, Flow Velocity, and Pipe Diameter. 2015. Available online: https://www.lorric.com/en/WhyLORRIC/Flowmeter/flow-rate-flow-velocity-pipe-diameter (accessed on 12 December 2015).
40. LI-COR. Pyranometer. 2015. Available online: https://www.licor.com/env/products/light/pyranometer (accessed on 4 July 2015).
41. CAS. dataTaker DT80. 2015. Available online: https://dataloggerinc.com/product/dt80-universal-input-data-logger/ (accessed on 4 July 2015).
42. Cooper, P. The absorption of radiation in solar stills. *Sol. Energy* **1969**, *12*, 333–346. [CrossRef]

43. El Khadraoui, A.; Bouadila, S.; Kooli, S.; Guizani, A.; Farhat, A. Solar air heater with phase change material: An energy analysis and a comparative study. *Appl. Therm. Eng.* **2016**, *107*, 1057–1064. [CrossRef]
44. Shukla, A.; Buddhi, D.; Sawhney, R.L. Solar water heaters with phase change material thermal energy storage medium: A review. *Renew. Sustain. Energy Rev.* **2009**, *13*, 2119–2125. [CrossRef]
45. Hossain, M.S.; Pandey, A.K.; Selvaraj, J.; Rahim, N.A.; Islam, M.M.; Tyagi, V.V. Two side serpentine flow based photovoltaic-thermal-phase change materials (PVT-PCM) system: Energy, exergy and economic analysis. *Renew. Energy* **2019**, *136*, 1320–1336. [CrossRef]
46. Hasan, A.; Alnoman, H.; Shah, A.H. Energy Efficiency Enhancement of Photovoltaics by Phase Change Materials through Thermal Energy Recovery. *Energies* **2016**, *9*, 782. [CrossRef]
47. Adnan, I.; Othman, M.Y.; Ruslan, M.H.; Alghoul, M.A.; Yahya, M.; Zaharim, A.; Sopian, K. Performance of Photovoltaic Thermal Collector (PVT) With Different Absorbers Design. ISSN: 1790-5079. *Wseas Trans. Environ. Dev.* **2009**, *5*, 321–330.
48. Hottel, H.C.; Whillier, A. Evaluation of flat-plate solar collector performance. *Trans. Conf. Use Sol. Energy* **1958**, *2*, 74.
49. Hossain, M.S.; Kumar, L.; Nahar, A. A Comparative Performance Analysis between Serpentine-Flow Solar Water Heater and Photovoltaic Thermal Collector under Malaysian Climate Conditions. *Int. J. Photoenergy* **2021**, *2021*, 7176506. [CrossRef]
50. Hossain, M.S.; Pandey, A.K.; Mohsin, A.T.; Jeyraj, S.; Kazi, E.H.; Rahim, N.A. Thermal and economic analysis of low-cost modified flat-plate solar water heater with parallel two-side serpentine flow. *J. Therm. Anal. Calorim.* **2015**, *123*, 793–806. [CrossRef]
51. Hossain, M.S.; Pandey, A.K.; Rahim, N.A.; Selvaraj, J.; Tyagi, V.V.; Islam, M.M. Self-cleaning assisted photovoltaic system with thermal energy storage: Design and performance evaluation. *Sol. Energy* **2020**, *206*, 487–498. [CrossRef]
52. Hossain, M.S.; Pandey, A.K.; Selvaraj, J.; Abd Rahim, N.; Rivai, A.; Tyagi, V.V. Thermal performance analysis of parallel serpentine flow based photovoltaic/thermal (PV/T) system under composite climate of Malaysia. *Appl. Therm. Eng.* **2019**, *153*, 861–871. [CrossRef]
53. Hossain, M.S.; Pandey, A.K.; Tunio, M.A.; Selvaraj, J.; Rahim, N.A. Chapter Ten—The Hybrid Solar Power/Wind System for Energy Production, Observation, Application, and Simulation. In *Clean Energy for Sustainable Development*; Academic Press: Cambridge, MA, USA, 2017; pp. 337–368. [CrossRef]
54. Hossain, M.S.; Saidur, R.; Fayaz, H.; Rahim, N.A.; Islam, M.R.; Ahamed, J.U.; Rahman, M.M. Review on solar water heater collector and thermal energy performance of circulating pipe. *Renew. Sustain. Energy Rev.* **2011**, *15*, 3801–3812. [CrossRef]
55. Ibrahim, A.; Fudholi, A.; Sopian, K.; Othman, M.Y.; Ruslan, M.H. Efficiencies and improvement potential of building integrated photovoltaic thermal (BIPVT) system. *Energy Convers. Manag.* **2014**, *77*, 527–534. [CrossRef]
56. Park, S.R.; Pandey, A.K.; Tyagi, V.V.; Tyagi, S.K. Energy and exergy analysis of typical renewable energy systems. *Renew. Sustain. Energy Rev.* **2014**, *30*, 105–123. [CrossRef]
57. Praveenkumar, S.; Agyekum, E.B.; Kumar, A.; Velkin, V.I. Thermo-enviro-economic analysis of solar photovoltaic/thermal system incorporated with u-shaped grid copper pipe, thermal electric generators and nanofluids: An experimental investigation. *J. Energy Storage* **2023**, *60*, 106611. [CrossRef]
58. Nahar, A.; Hasanuzzaman, M.; Rahim, N.A. Numerical and experimental investigation on the performance of a photovoltaic thermal collector with parallel plate flow channel under different operating conditions in Malaysia. *Sol. Energy* **2017**, *144*, 517–528. [CrossRef]
59. Rahman, M.M.; Hasanuzzaman, M.; Rahim, N.A. Effects of operational conditions on the energy efficiency of photovoltaic modules operating in Malaysia. *J. Clean. Prod.* **2017**, *143*, 912–924. [CrossRef]
60. Sardarabadi, M.; Passandideh-Fard, M.; Zeinali Heris, S. Experimental investigation of the effects of silica/water nanofluid on PV/T (photovoltaic thermal units). *Energy* **2014**, *66*, 264–272. [CrossRef]
61. Islam, M.M.; Hasanuzzaman, M.; Rahim, N.A.; Pandey, A.K.; Rawa, M.; Kumar, L. Real time experimental performance investigation of a NePCM based photovoltaic thermal system: An energetic and exergetic approach. *Renew. Energy* **2021**, *172*, 71–87. [CrossRef]
62. Kline, S.J. Describing uncertainty in single sample experiments. *J. Mech. Eng.* **1953**, *75*, 3–8.
63. Taylor, J. *Introduction to Error Analysis, the Study of Uncertainties in Physical Measurements*, 2nd ed.; University Science Books: New York, NY, USA, 1997.
64. Kumar, S.; Tiwari, G.N. Life cycle cost analysis of single slope hybrid (PV/T) active solar still. *Appl. Energy* **2009**, *86*, 1995–2004. [CrossRef]
65. Leland, T.B.; Anthony, J.T. *Engineering Economy Book*, 4th ed.; McGraw Hill: New York, NY, USA, 1998; pp. 46–161. ISBN 0-070-115964-9.
66. Ammar, A.M.A.-T.; Megat, M.H.; Kamaruzzaman, S.; Wahab, M.A. An Economical Analysis for a Stratified Integrated Solar Water Heater with a Triangular Shape. *J. Adv. Sci. Arts* **2009**, *1*, 17–28.
67. Preet, S.; Bhushan, B.; Mahajan, T. Experimental investigation of water based photovoltaic/thermal (PV/T) system with and without phase change material (PCM). *Sol. Energy* **2017**, *155*, 1104–1120. [CrossRef]
68. Yang, X.; Sun, L.; Yuan, Y.; Zhao, X.; Cao, X. Experimental investigation on performance comparison of PV/T-PCM system and PV/T system. *Renew. Energy* **2018**, *119*, 152–159. [CrossRef]
69. Al Imam, M.F.I.; Beg, R.A.; Rahman, M.S.; Khan, M.Z.H. Performance of PVT solar collector with compound parabolic concentrator and phase change materials. *Energy Build.* **2016**, *113*, 139–144. [CrossRef]

70. Hosseinzadeh, M.; Sardarabadi, M.; Passandideh-Fard, M. Energy and exergy analysis of nanofluid based photovoltaic thermal system integrated with phase change material. *Energy* **2018**, *147*, 636–647. [CrossRef]
71. PraveenKumar, S.; Agyekum, E.B.; Kumar, A.; Velkin, V.I. Performance evaluation with low-cost aluminum reflectors and phase change material integrated to solar PV modules using natural air convection: An experimental investigation. *Energy* **2023**, *266*, 126415. [CrossRef]